

DOI: 10.1002/sml.200700378

# Size-Dependent Cytotoxicity of Gold Nanoparticles

Yu Pan, Sabine Neuss, Annika Leifert, Monika Fischler, Fei Wen, Ulrich Simon,\* Günter Schmid, Wolfgang Brandau, and Willi Jahnen-Dechent\*

**G**old nanoparticles are widely used in biomedical imaging and diagnostic tests. Based on their established use in the laboratory and the chemical stability of Au<sup>0</sup>, gold nanoparticles were expected to be safe. The recent literature, however, contains conflicting data regarding the cytotoxicity of gold nanoparticles. Against this background a systematic study of water-soluble gold nanoparticles stabilized by triphenylphosphine derivatives ranging in size from 0.8 to 15 nm is made. The cytotoxicity of these particles in four cell lines representing major functional cell types with barrier and phagocyte function are tested. Connective tissue fibroblasts, epithelial cells, macrophages, and melanoma cells prove most sensitive to gold particles 1.4 nm in size, which results in IC<sub>50</sub> values ranging from 30 to 56 μM depending on the particular 1.4-nm Au compound–cell line combination. In contrast, gold particles 15 nm in size and Tauredon (gold thiomalate) are nontoxic at up to 60-fold and 100-fold higher concentrations, respectively. The cellular response is size dependent, in that 1.4-nm particles cause predominantly rapid cell death by necrosis within 12 h while closely related particles 1.2 nm in diameter effect predominantly programmed cell death by apoptosis.

## Keywords:

- cell growth
- cytotoxicity
- gold
- nanoparticles
- toxicology

[\*] Y. Pan, Prof. W. Jahnen-Dechent  
Biomedical Engineering, Biointerface Laboratory  
RWTH Aachen University  
Pauwelsstrasse 30, 52074 Aachen (Germany)  
Fax: (+49) 241-80-82573  
E-mail: willi.jahnen@rwth-aachen.de

Dr. S. Neuss  
Pathology  
RWTH Aachen University (Germany)

A. Leifert, Dr. M. Fischler, Dr. F. Wen, Prof. U. Simon  
Inorganic Chemistry  
RWTH Aachen University (Germany)  
Fax: (+49) 241-809-9003  
E-mail: ulrich.simon@ac.rwth-aachen.de

Prof. G. Schmid  
Inorganic Chemistry  
University of Duisburg-Essen (Germany)

Prof. W. Brandau  
Radiochemistry, University Hospital Essen (Germany)

 Supporting information for this article is available on the WWW under <http://www.small-journal.com> or from the author.

## 1. Introduction

Nanoscale materials hold great promise for both industrial and biomedical applications. Toxicological studies suggest that nanoparticles may cause adverse health effects, but the fundamental cause–effect relationships are ill defined. Thus, the interaction of nanoparticles with biological systems including living cells has become one of the most urgent areas of collaborative research in materials science and biology.<sup>[1]</sup> The most interesting properties of nanoparticles, that is, the quantum size effect or surface-induced effects, result from their minute size. Nanoparticles are of similar size to typical cellular components and proteins, and thus may bypass natural mechanical barriers, possibly leading to adverse tissue reaction. The primary interaction site of cells and particles smaller than about 100 nm is the pericellular space in and around the microcapillaries. Opsonization, the binding of blood components to the particles, greatly facilitates endocytosis. Opsonins mediate material–cell receptor interactions and enhance endocytosis. Con-

versely, the surface chemistry of particles can control opsonization, thus facilitating or preventing endocytosis. Charged or hydrophobic particles adsorb serum proteins easily while particles covered with antifouling polymers, such as polyethylene glycol, can resist opsonization, effectively creating “stealth particles” with extended circulation times.

Phagocytosis is prevalent in professional phagocytes of the monocyte/macrophage lineage including dendritic cells and osteoclasts. Endothelial cells likewise possess a highly evolved machinery to endocytose large and small particles. Once the particles are endocytosed, they may be degraded in the endolysosomal compartment. Innoxious but nondegradable matter may eventually be excreted in feces or exhaled by the lung along with the phagocytosing cells. Failure of degradation or excretion may result in chronic inflammation, ultimately leading to severe tissue damage. Endocytosis of nanomaterials can trigger the binding of nanoparticles to intracellular targets, which causes disturbance of cellular signaling, motility, and metabolism.

Gold nanoparticles were variously described as nontoxic<sup>[2]</sup> or toxic.<sup>[3,4]</sup> Gold nanoparticles are used as tracers<sup>[5]</sup> and the cellular trajectories change according to the biological signals added to the bulk material, again suggesting that gold particles by themselves are nontoxic.<sup>[6]</sup> Furthermore, oligonucleotide-modified 13-nm gold particles were applied to intracellular gene regulation.<sup>[7]</sup> An entire anti-inflammatory type of therapy, chrysotherapy, actually relies on gold complexes. A recent report elaborated that gold(III) salts attenuate antigen presentation and thus reduce autoimmune reactions in rheumatoid arthritis,<sup>[8]</sup> which suggests a molecular mechanism for the anti-inflammatory/anti-rheumatoid arthritis activity of gold drugs such as Auranofin or Tauredon.

Based on *in vitro* investigations of the interaction of water-soluble  $\text{Au}_{55}[\text{Ph}_2\text{PC}_6\text{H}_4\text{SO}_3\text{H}(\text{Na})]_{12}\text{Cl}_6$  with natural B-DNA and molecular modeling studies, we found that the 1.4-nm  $\text{Au}_{55}$  cluster cores bound to the major groove with high selectivity and stability. This binding event was accompanied by a partial substitution of triphenylphosphine monosulfonate (TPPMS) for negatively charged phosphates of the DNA, which most likely bound the gold nanoparticles due to the high electronegativity of the metal.<sup>[9]</sup> Hypothetically, this could result in a general blockade of transcription. This mechanism would require a rather stringent size limitation, because clusters, characteristically smaller or larger than the 1.4-nm  $\text{Au}_{55}$  clusters, would be less likely to interact with B-DNA in such a way for steric reasons. From these former experiments it is also known that sulfonated triphenylphosphines do not show visible toxicity under the same conditions. These results prompted us to start a series of cell-based experiments, in which the gold-cluster compound showed lower  $\text{IC}_{50}$  values (inhibitory concentrations that effected 50% growth inhibition) than the well-established cytostatic agent, cisplatin, for different human cancer cells.<sup>[10]</sup> From [ $^{198}\text{Au}$ ]gold radioanalysis of cell fractions we deduced that 20–25% of the gold was associated with DNA-containing fractions of the nucleus, which is in accordance with the *ex vivo* experiments mentioned above.

Gold nanoparticles are readily endocytosed by mammalian cells and the kinetics and saturation depend upon the physical dimensions of the nanoparticles.<sup>[11]</sup> Pernodet and colleagues reported that with the presence of intracellular gold nanoparticles  $13 \pm 1$  nm in size, actin stress fibers disappeared and major adverse effects on cell viability were induced.<sup>[4]</sup> Gold nanoparticles  $3.5 \pm 0.7$  nm in diameter capped by lysine and poly-L-lysine were biocompatible and nonimmunogenic.<sup>[12]</sup> Cysteine- and citrate-capped 4-nm gold nanoparticles, glucose-reduced 12-nm nanoparticles, and citrate-, biotin-, and cetyltrimethylammonium bromide-capped 18-nm gold nanoparticles were all endocytosed without signs of cytotoxicity.<sup>[2]</sup> Studies from Goodman and co-workers demonstrated that cationic gold nanoparticles were moderately toxic, whereas anionic gold nanoparticles were nontoxic.<sup>[3]</sup> A pilot study from our own laboratory showed that  $\text{Au}_{55}$  clusters stabilized with TPPMS of diameter 1.4 nm ( $\text{Au}1.4\text{MS}$ ) were more toxic than cisplatin in a range of cell lines.<sup>[10]</sup> Thus, conflicting yet not necessarily contradictory data exist with regard to the toxicity of gold nanoparticles.

Herein, we studied the influence of particle size on cytotoxicity. To this end, we varied the Au cluster size from 0.8 up to 15 nm. We studied the stability of the nanoparticles in a complex, high-ionic-strength aqueous environment containing macromolecules mimicking blood. Typically this is achieved by a serum-containing cell-culture medium, which may affect stability, solubility, and hydrophobicity. We confronted the nanoparticles with various cell types representing the principal barriers and lining cells of the body (epithelial and endothelial cells), phagocytes (macrophages), and tissue stromal cells (connective tissue fibroblasts). Cells are generally most vulnerable during proliferation and tend to be more stress-tolerant in the quiescent state. Thus, we tested cytotoxicity in both actively dividing cells in the logarithmic growth phase and quiescent cells in the stationary phase. In summary, we describe the comparative cytotoxicity testing in a 96-well plate-based cell assay of gold compounds including a commercial drug and gold nanoparticles of varying size.

## 2. Results and Discussion

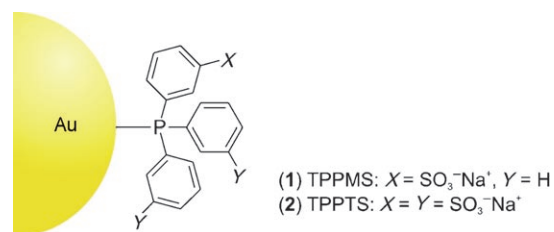
### 2.1. Au Nanoparticle Synthesis and Stability in Media

We varied the size of Au nanoparticles from 0.8 to 15 nm. To exclude the influence on toxicity of various ligands protecting the different nanoparticles, we used  $\text{Ph}_2\text{PC}_6\text{H}_4\text{SO}_3\text{Na}$  (TPPMS) throughout, except in one case where tris-sulfonated triphenylphosphine  $\text{P}(\text{C}_6\text{H}_4\text{SO}_3\text{Na})_3$  (TPPTS) was used for comparison. The statements of size used in the following relate to the diameter of the gold core. We use the abbreviations MS and TS for the mono- and trisubstituted ligands, respectively, and formulae such as  $\text{Au}1.4\text{MS}$  for the clusters stabilized by TPPMS.

The synthesis of the cluster  $\text{Au}0.8\text{MS}$  is described in the Experimental Section. It represents a water-soluble TPPMS derivative of the fully characterized compound  $\text{Au}_9(\text{PPh}_3)_8(\text{NO}_3)_2$ .<sup>[13]</sup>  $\text{Au}1.4\text{MS}$  represents the likewise well-defined

and characterized compound  $\text{Au}_{55}(\text{Ph}_2\text{PC}_6\text{H}_4\text{SO}_3\text{Na})_{12}\text{Cl}_6$ , which is extensively described in the literature<sup>[14,15]</sup> and is a derivative of the well-known and fully characterized cluster compound  $\text{Au}_{55}(\text{PPh}_3)_{12}\text{Cl}_6$ .<sup>[16–18]</sup>  $\text{Au}_{1.4}\text{TS}$  was synthesized in an analogous manner to  $\text{Au}_{1.4}\text{MS}$  (see Experimental Section).  $\text{Au}_{1.2}\text{MS}$  and  $\text{Au}_{1.8}\text{MS}$  are available from Strem Chemicals, Newburyport.<sup>[19]</sup> Contrary to the stoichiometric  $\text{Au}_{0.8}\text{MS}$  and  $\text{Au}_{1.4}$  clusters,  $\text{Au}_{1.2}\text{MS}$  and  $\text{Au}_{1.8}\text{MS}$  exhibit size distributions of about  $\pm 0.2$  nm derived from transmission electron microscopy (TEM) measurements. Thus, a stoichiometric formula cannot be given. However, it can be estimated that the average-sized  $\text{Au}_{1.2}\text{MS}$  particles consist of  $\approx 35$  Au atoms and the  $\text{Au}_{1.8}\text{MS}$  particles of  $\approx 150$  Au atoms. The number of TPPMS ligands corresponds exactly to the number of Au atoms, that is, the Au/ligand ratio is 1:1, which indicates that the clusters are capped by more than one monolayer of the ligand molecules. Gold nanoparticles in the size range of 15 nm were prepared by following the citrate method of Turkevitch.<sup>[20]</sup> The citrate layer on the particle surface was replaced by TPPMS as described.<sup>[21]</sup> From numerous TEM investigations it is known that the size distribution of these colloidal species is generally within  $15 \pm 1.5$  nm.

Scheme 1 shows a model of a triphenylphosphine-capped gold nanoparticle and Table S1 (Supporting Information) lists key features of the nanoparticles used in this study, as determined in previous studies or as provided by the manufacturer.



**Scheme 1.** Model of Au cluster with the triphenylphosphine derivative ligand. Not drawn to size.

We tested the stability of the materials in the serum-containing cell-culture media formulated for proper growth of the cell lines used in this study. We reasoned that the medium composition might affect particle aggregation and that aggregation of materials would greatly influence the endocytic pathway and ultimately the cellular trajectories of materials precluding or favoring intracellular targets. Figure S1 (Supporting Information) shows macroscopic and microscopic aspects of medium–material combinations in the absence of any cells. Materials were grouped according to their stability in specific media and over time. A synopsis of the aggregation behavior of Au compounds is given in Table S2 (Supporting Information).

## 2.2. Cytotoxicity Testing of Au Nanoparticles

We added Au compounds to HeLa cervix carcinoma epithelial cells (termed HeLa), SK-Mel-28 melanoma cells

(SK-Mel-28), L929 mouse fibroblasts (L929), and mouse monocytic/macrophage cells (J774A1) and first studied their response by optical and electron microscopy. Figure 1 shows representative microphotographs of HeLa cells that depict the time course of treatment with  $\text{Au}_{1.4}\text{MS}$  (Figure 1A–F) and of J774A1 cells treated with the compounds indicated (Figure 1G–L). HeLa cells, like SK-Mel-28 and L929 cells (not shown), formed tight monolayers in the absence of Au compounds (Figure 1A,B). Figure 2C and D represent optical and electron microscopic views of HeLa cells, respectively, after 1 h of treatment with  $\text{Au}_{1.4}\text{MS}$ . The cells were swollen and started losing substrate contact. TEM showed membrane blebbing and vesicle formation at the plasma membrane, which suggests strong activation of the cells (Figure 1D). At a treatment time of 12 h (Figure 1E,F) the cells were strongly swollen, had fragmented nuclei, and many cells had lost both cell-to-cell and cell-to-substrate contact. The few cells that remained attached to the culture dish showed cytoplasmic disorganization, nuclear fragmentation, and membrane blebbing, thus indicating apoptosis and secondary necrosis. Figure 1G–L shows optical micrographs of J774A1 macrophages treated for 1 h with Au compounds as indicated. As in HeLa cells, strong membrane blebbing was observed in treated (Figure 1H–L) but not in untreated J774A1 cells (Figure 1G). J774A1 cells treated with  $\text{Au}_{15}\text{MS}$  particles had engorged themselves with the particles (Figure 1K). Collectively the microscopic data presented in Figure 1 show that the cells had endocytosed Au particles and showed signs of activation and severe stress, including apoptosis and secondary necrosis, after treatment with  $\text{Au}_{1.4}\text{MS}$  clusters.

We quantified the toxicity of Au compounds in four cell lines by determining the  $\text{IC}_{50}$  values in MTT assays ( $\text{MTT} = 3$ -(4,5-dimethylthiazol-2-yl)-2,5-diphenyltetrazolium bromide). We reasoned that cells actively growing and dividing during logarithmic growth should be more vulnerable to toxic insults than cells near or at the stationary phase of cell culture. Thus, we determined growth curves for all cell lines to estimate the logarithmic and stationary growth phases in relation to the number of cells seeded into each well of a 96-well cell-culture plate. Figure 2 shows the growth curves for all four cell lines maintained in the media detailed in the Experimental Section. This graph served as a reference to estimate whether cells were in the logarithmic or stationary phase of cell culture at the start of any given experiment.

## 2.3. Au Nanoparticles Cause Size-Dependent Cell Death

Having established growth characteristics for the reporter cell lines, we treated the cells with Au compounds for up to 48 h to observe the full effect of toxicity. Given the strong reaction of cells to  $\text{Au}_{1.4}\text{MS}$  (and  $\text{Au}_{1.4}\text{TS}$ ) illustrated in Figure 1C–F, this incubation time should reliably detect even low or slow-acting toxicity and vice versa. We performed toxicity tests during both the logarithmic and stationary phases of cell growth following the time course depicted in Figure 2E and F. Invariably cells during the logarithmic growth phase proved 1.5–3.3-fold more sensitive to

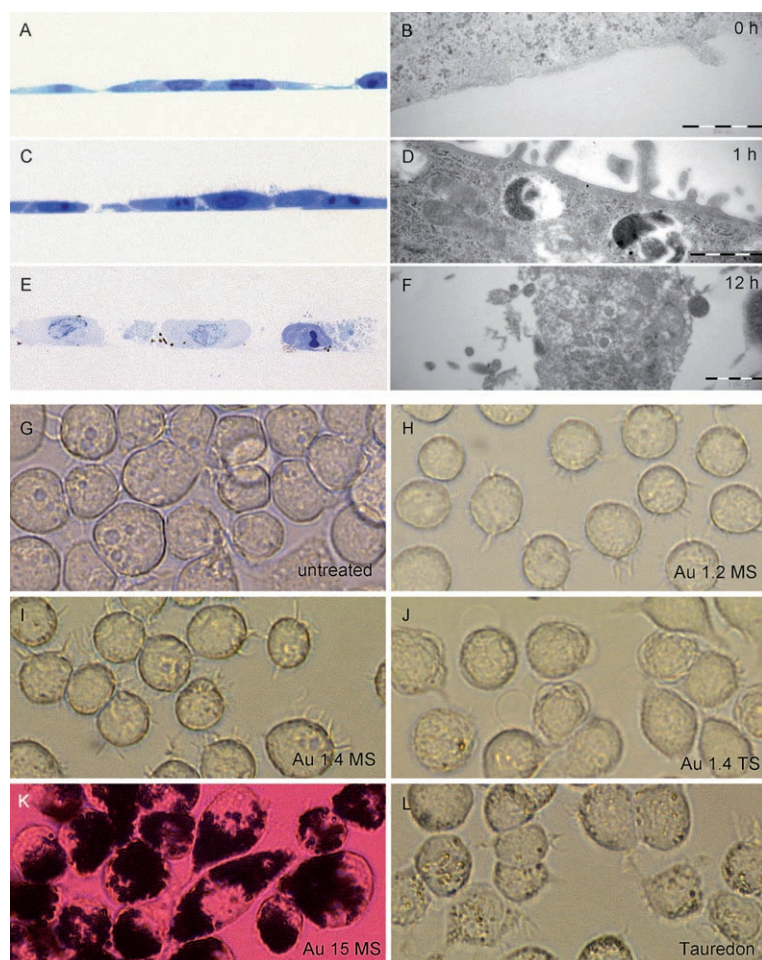


**Figure 1.** Microscopic views of HeLa (A–F) and J774A1 cells (G–L) treated with Au compounds as indicated. A–F) HeLa cells were treated for 0, 1, or 12 h with Au1.4MS clusters. Cells were fixed, flat embedded, turned by 90°, and mounted on stubs for semithin and ultrathin sectioning to reveal a cross-sectional view of the monolayer. Sections were stained and viewed with an optical microscope using an X40 lens (A, C, E) or with an electron microscope (B, D, F). Optical micrographs show a 200- $\mu\text{m}$  sector of the monolayer; scale bars in the TEM images indicate 0.5  $\mu\text{m}$  (0 h) or 1  $\mu\text{m}$  (1 and 12 h). G–L) J774A1 macrophages were treated for 1 h as indicated and viewed live using an inverted optical microscope and an X40 lens. The width of each micrograph equals 200  $\mu\text{m}$ . Colloidal Au 15-nm particles stained the endocytic compartment of the cells black (K) sparing the nucleus. The background hue is due to the color of dissolved materials.

toxic compounds than during the stationary phase (data not shown). In the following figures, however, we only list  $\text{IC}_{50}$  values derived from cells in the logarithmic growth phase for clarity of presentation.

A typical experiment measuring the cytotoxicity of Au compounds in logarithmic-phase HeLa cells is illustrated in Figure 3A. Gold clusters Au1.4MS and Au1.4TS proved most toxic in this assay with  $\text{IC}_{50}$  values of 46 and 30  $\mu\text{m}$ , respectively. Surprisingly, Au clusters of even moderately different size stabilized with the same TPPMS ligand, Au0.8MS ( $\text{IC}_{50}$  250  $\mu\text{m}$ ), Au1.2MS ( $\text{IC}_{50}$  140  $\mu\text{m}$ ), and Au1.8MS ( $\text{IC}_{50}$  230  $\mu\text{m}$ ), were four- to sixfold less toxic. Despite obvious endocytosis by the cells (see Figure 1K for example), the colloidal compound Au15MS was completely nontoxic up to 6300  $\mu\text{m}$ . Higher concentrations of this compound were not tested because of solubility issues. Likewise Tauredon (gold thiomalate) scored nontoxic in all cells

tested at concentrations up to 10 mM except in J774A1 cells, which proved more sensitive ( $\text{IC}_{50} \approx 600 \mu\text{m}$ ).

Taken together these results suggest a stringent size dependency of the cytotoxicity of nanoscopic gold clusters. The toxicity was independent of whether TPPMS or TPPTS was used to stabilize the Au1.4 cluster.  $\text{IC}_{50}$  values of both compounds were virtually identical in HeLa cells and very similar across the four cell lines tested, ranging from 30  $\mu\text{m}$  in J774A1 macrophages to 56  $\mu\text{m}$  in L929 fibroblasts (Figure 3B). We also conclude that ligand toxicity did not contribute to the overall cluster toxicity, because both Au1.4MS and Au1.4TS clusters had almost identical  $\text{IC}_{50}$  values. Furthermore, the Au1.4 clusters contained 12 ligand molecules per 55 Au atoms, which suggests  $\approx 10 \mu\text{m}$  ligand at the  $\text{IC}_{50}$  value of Au1.4MS and Au1.4TS. Figure 3A shows that both ligands were nontoxic at this low concentration. In addition, Au0.8, Au1.2, and Au1.8 clusters all contained equimolar amounts of Au and ligand (see Table S1, Supporting Information), but were nontoxic at concentrations even higher than Au1.4 clusters. In

summary, these data strongly suggest that the size of 1.4 nm and not the ligand chemistry was the chief determinant of toxicity of the Au clusters.

#### 2.4. Apoptosis Versus Necrosis Caused by Au Clusters

Next we asked what kind of cell death Au clusters cause. Basically two kinds of cell death are known. Fast-acting metabolic poisons and strong physical stress, such as freezing, boiling, or shearing, rupture cell membranes and cause rapid cell necrosis. The contents released by necrotic cells are highly inflammatory and therefore necrotic cells invariably cause inflammation in the body. In contrast, a slow-acting form of cell death called apoptosis does not involve membrane damage and inflammation. During apoptosis or programmed cell death, cells undergo an energy-dependent

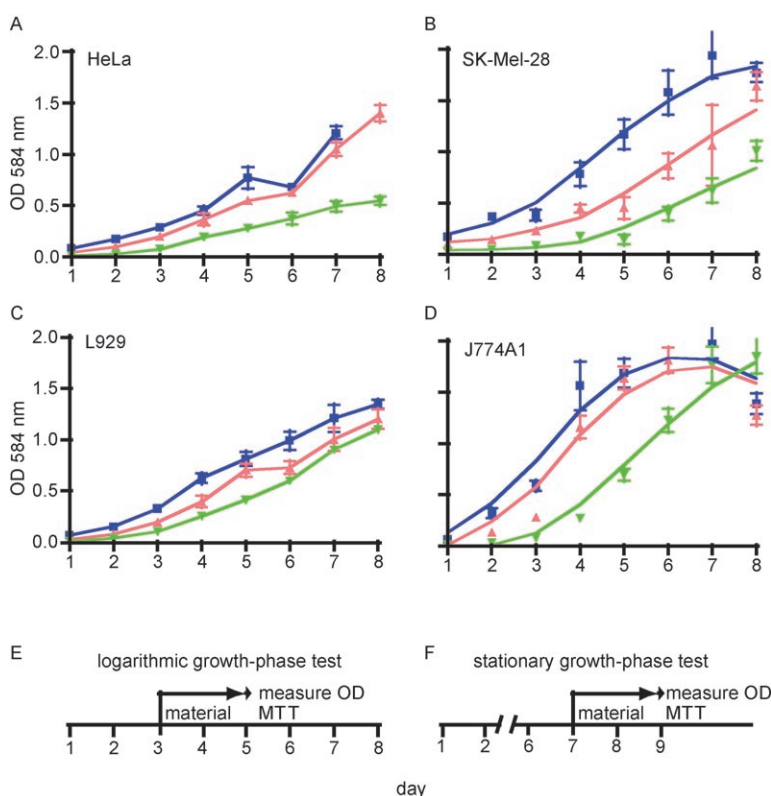


**Figure 2.** A–D) Cell-growth curves using different cell-plating numbers and the indicated cell lines. The initial cell number was 1000 (green), 2000 (red), or 4000 cells (blue) seeded into each well of a 96-well tissue-culture plate. E, F) Protocol of cytotoxicity testing starting during the logarithmic (E) or stationary growth phase (F). OD = optical density.

sequence of events, ultimately fragmenting nuclei and cytoplasmic organelles into small membrane-sealed apoptotic bodies that can be cleared by phagocytes. Apoptosis is the body's default pathway of clearing dead cells or cells marked for destruction. Membrane blebbing and vesicle formation as observed in Figure 1D are typical of apoptosis. A salient diagnostic feature of apoptosis is, however, externalization of the membrane lipid phosphatidylserine (PS) to the outer leaflet of the cell membrane. We double stained cells with annexin V (aV) for externalized PS as a measure of apoptosis and with the nuclear stain propidium iodide (PI) as an indicator of membrane integrity and thus necrosis. A typical view of healthy cells and of necrotic cells treated with 110  $\mu\text{M}$  Au1.4MS is shown in Figure 4. Untreated cells did not expose PS on their external plasma membrane leaflet and stained double negative for aV and PI (Figure 4A,B). In contrast, necrotic cells stained double positive, green for aV and red for PI (Figure 4C,D).

To estimate if the cytotoxic Au compounds caused preferentially apoptotic or necrotic cell death, we treated HeLa cells in the logarithmic growth phase with the pro-apoptotic compound staurosporine as a positive control substance or with Au1.2MS or Au1.4MS, two cytotoxic Au cluster compounds varying only slightly in size. The cells were double stained with aV and PI and subjected to flow cytometry (Figure 5). Signals were gated for high forward and side-

ward scattering (FSC and SSC, respectively) to separate intact cells from particles and cell fragments. The gated signals formed four groups: aV/PI double negative, intact live cells; aV positive/PI negative, apoptotic cells; aV positive/PI positive, necrotic cells; and a very low fraction of aV negative/PI positive, large nuclear fragments.

Figure 6 shows a compilation of a representative experiment detailing the relative amounts of live, necrotic, and apoptotic HeLa cells after treatment for 6, 12, 18, and 24 h with buffer only (untreated), staurosporine, Au1.2MS, or Au1.4MS. As expected, untreated cells remained live, nonapoptotic and nonnecrotic at all time points. The positive control staurosporine effected mostly apoptosis, but a small fraction of aV/PI double positive cells was also detected, which indicated secondary necrosis especially at later time points. The analysis revealed a striking difference in the cytotoxic capacity of Au1.2MS and Au1.4MS that was not noted from the  $\text{IC}_{50}$  measurements at 48 h. Interestingly, the smaller cluster compound Au1.2MS at 140  $\mu\text{M}$  caused cell death in about 50% of all cells after treatment for 24 h with an almost equal proportion of apoptotic and secondary necrotic cells, thus indicating relatively lower cytotoxicity and slow killing. In contrast, 110  $\mu\text{M}$  Au1.4MS caused cell death in 70% after 12 h and in over 90% after 24 h with a transient population of apoptotic cells and a steady increase in secondary necrotic cells. We take this as evidence for a much faster and more efficient cytotoxic action of Au1.4MS versus Au1.2MS, despite a similar concentration and their close chemical and physical similarity. Note that this important difference in action was only revealed in the kinetic analysis, and not in the traditional endpoint analysis for determining the  $\text{IC}_{50}$  values.

We repeated the experiment for Au1.2MS and Au1.4MS with twice the  $\text{IC}_{50}$  concentration previously determined by endpoint analysis (Figure 3B). Figure S2 (Supporting Information) shows an extension of the experiment depicted in Figure 6C and D. This experimental setup fully confirmed the previous results, in that Au1.2MS was markedly less cytotoxic than Au1.4MS despite a threefold higher concentration.

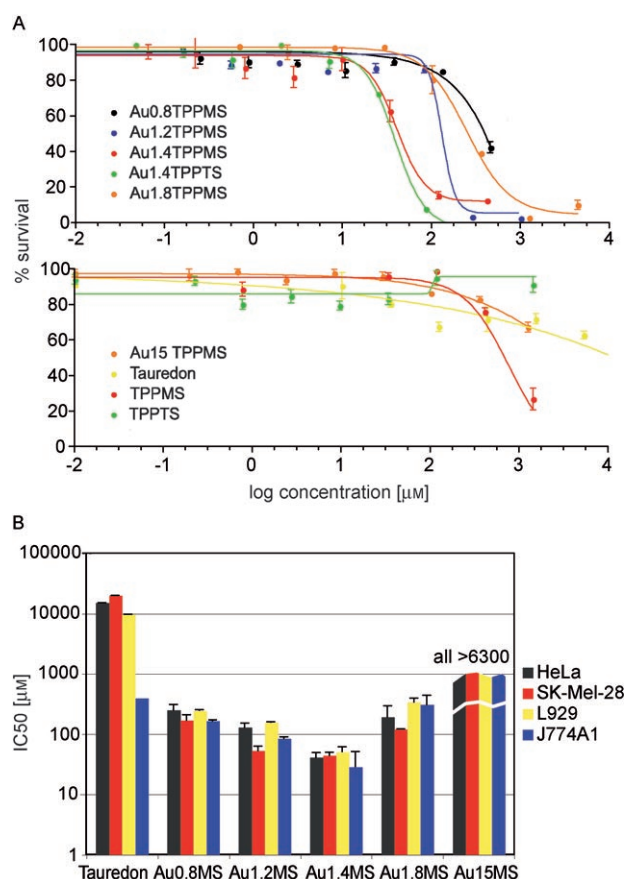


**Figure 3.** Cytotoxicity of Au compounds during the logarithmic growth phase of four cell lines. A) HeLa cells were seeded at 2000 cells/well and grown for 3 days into the logarithmic growth phase. Au compounds were added for 48 h and MTT tests were performed as detailed in the Experimental Section. The logarithmic curve fits of tabulated MTT readings are shown. Each data point represents the mean  $\pm$  standard error (SE) of sample triplicates. B) Note that the IC<sub>50</sub> values of Au1.4MS were lowest across all cell lines and that Au compounds of smaller or larger size were progressively less cytotoxic, which suggests a stringent size dependency of cytotoxicity. All concentrations relate to the amount of gold detected by atomic-absorption spectroscopy (AAS) in the authentic samples *after* performing the cytotoxicity test. This procedure ruled out the possibility that cluster synthesis contaminants or dilution errors may have caused erroneous results.

### 3. Conclusions

We have defined the size range, concentration range, type of cell culture, and treatment time as important basic parameters to unravel the exact trajectory and molecular targets of Au nanoclusters. These clusters constitute a novel class of tunable nanoscale materials with potential medical application as cytostatic agents that preferably promote apoptosis or secondary necrosis depending predominantly on their size.

The cytotoxicity of TPPMS/TPPTS-modified gold nanoparticles depended primarily on their size and not on ligand chemistry. Particles 1–2 nm in size were highly toxic and both smaller gold compounds (Tauredon) and larger 15-nm gold colloids were comparatively nontoxic, irrespective of

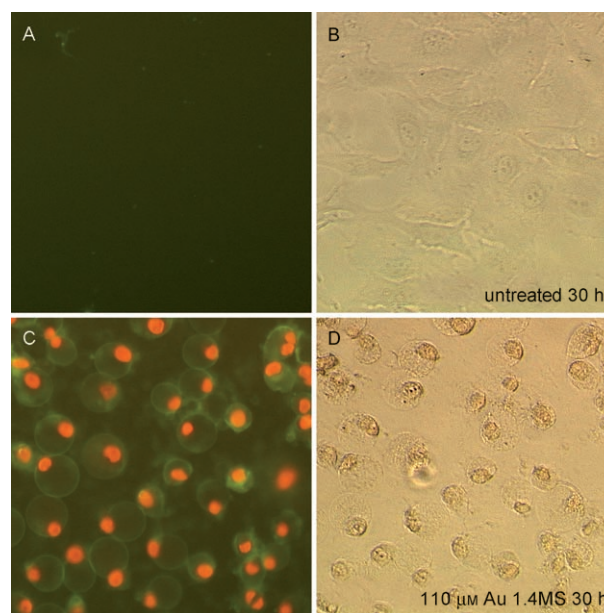


**Figure 4.** Fluorescent staining of HeLa cells with aV for apoptosis (green fluorescence) and PI for necrosis (red fluorescence). Untreated cells stained negative. Cells treated with 110  $\mu\text{M}$  Au1.4MS for 30 h underwent apoptosis and secondary necrosis and thus stained double positive. Note that the treated cells also rounded up and detached from the culture dish.

the cell type tested. Differences in the kind of cell death pathway (apoptosis versus necrosis) were consistently observed. This finding suggests different uptake kinetics and/or cellular target specificities even for similarly sized gold nanoparticles. Most likely nanoparticle toxicity follows endocytosis, but it is entirely possible that the toxicity may stem from interactions at the cell membrane, even though the particles are also endocytosed.

## 4. Experimental Section

**Synthesis and stability of gold nanoparticles:** AuPPh<sub>3</sub>Cl, benzene, BF<sub>3</sub>·OEt<sub>2</sub>, CH<sub>2</sub>Cl<sub>2</sub>, diethylene glycol dimethyl ether, ethanol, HAuCl<sub>4</sub>·3 H<sub>2</sub>O, H<sub>2</sub>SO<sub>4</sub>, NaBH<sub>4</sub>, PPh<sub>3</sub>, sodium citrate dihydrate, and TPPTS were purchased from diverse suppliers. All chemicals were used as received, and H<sub>2</sub>O was obtained from a Purelab Plus water purification system. TPPMS was synthesized as described.<sup>[22]</sup>

**Au0.8MS:** The Au<sub>9</sub>(PPh<sub>3</sub>)<sub>8</sub>(NO<sub>3</sub>)<sub>3</sub> cluster was synthesized as published.<sup>[23]</sup> The single-crystal structure was described previously.<sup>[13]</sup> To transfer the cluster into the aqueous phase, a solution of TPPMS (1.1 mg,  $2.8 \times 10^{-3}$  mmol) in H<sub>2</sub>O (0.5 mL) was added to a solution of Au<sub>9</sub>(PPh<sub>3</sub>)<sub>8</sub>(NO<sub>3</sub>)<sub>3</sub> cluster (1.3 mg,  $3.2 \times 10^{-4}$  mmol) in CH<sub>2</sub>Cl<sub>2</sub> (0.5 mL), and the mixture was stirred at room temperature until the organic phase was colorless. After centrifugation, the red supernatant was ready for further use. The obtained water-soluble cluster solution showed a single resonance in <sup>31</sup>P{<sup>1</sup>H} NMR spectra at  $\delta = 54.5$  ppm in D<sub>2</sub>O, which is

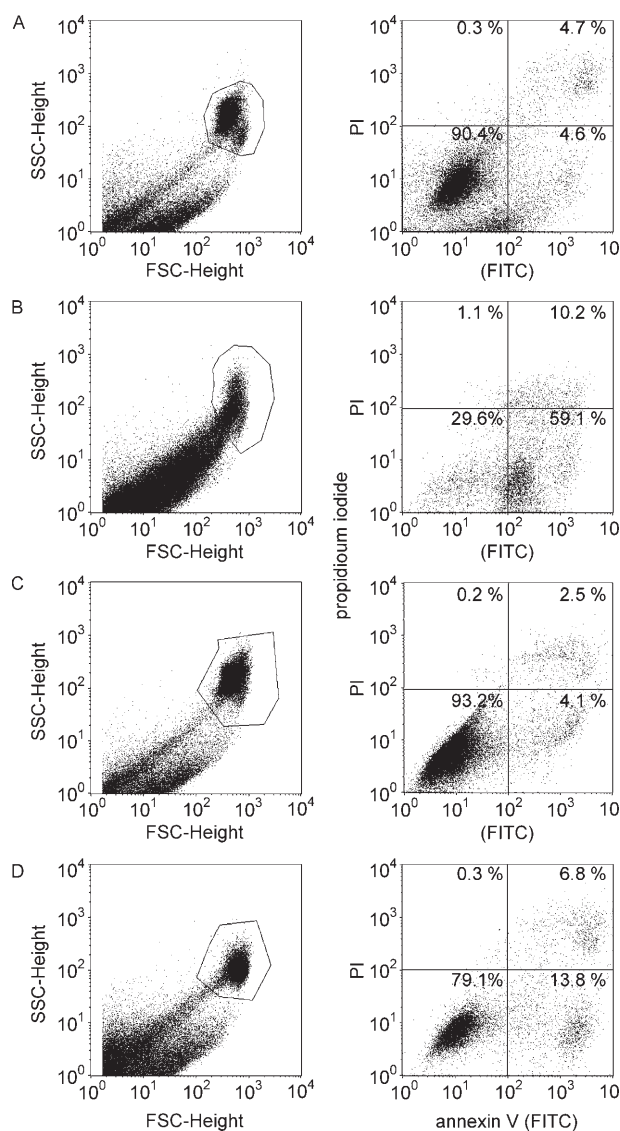


**Figure 5.** Determination of live, apoptotic, and necrotic HeLa cells treated with test compounds for 6 h. Cells were analyzed by flow cytometry and gated as shown in the left-hand panels. Gated cells were scored for aV/PI double staining (right panels) to estimate the relative amounts of live cells (aV/PI double negative, bottom-left quadrant), apoptotic cells (aV positive/PI negative, bottom-right quadrant), and necrotic cells (aV/PI double positive, top-right quadrant). The percentages of cells are given for each quadrant. A) HeLa untreated; B) HeLa, 2  $\mu\text{M}$  staurosporine, 6 h; C) HeLa, 140  $\mu\text{M}$  Au1.2MS, 6 h; D) HeLa, 110  $\mu\text{M}$  Au1.4MS, 6 h.

in good agreement with the data obtained from the  $\text{CH}_2\text{Cl}_2$ -soluble  $\text{Au}_8(\text{PPh}_3)_8(\text{NO}_3)_2$  cluster compound.<sup>[24]</sup> Furthermore, the UV/Vis spectrum of the cluster in aqueous solution was found to be consistent with that of the  $\text{Au}_8$  core reported elsewhere.<sup>[25]</sup>

**Au1.4TS:** Au1.4TS was synthesized analogously to Au1.4MS (see Ref. [20]), except that the two-phase system was stirred for 10 days instead of 3 days to achieve full ligand exchange.

**Au15MS:** Citrate-stabilized gold colloids were synthesized by following a published protocol.<sup>[20]</sup> For ligand exchange, TPPMS (1 mg per 10 mL of a 0.4 mM solution referring to Au) was added to the red solution. The mixture was stirred for 5 min and kept at

4 °C overnight. To increase the concentration and remove excess ligand, the solution was centrifuged to obtain a dark red solution. The UV/Vis spectrum showed an absorption maximum at 527 nm.

Au1.2MS and Au1.8MS were kindly provided and characterized by Strem Chemicals, Newburyport.<sup>[19]</sup>

Stability tests were performed in 96-well microtiter plates. For each test, water-dissolved material (20  $\mu\text{L}$ ) was added to the medium (50  $\mu\text{L}$ ). Materials dissolved in culture media were analyzed microscopically after 5 min and 12 h.

**Cell culture and cytotoxicity assays:** Four cell lines, SK-Mel-28 human melanoma, HeLa human cervix carcinoma, L929 mouse fibroblasts, and J774A1 mouse macrophages, were used in this study. SK-Mel-28 and J774A1 cells were maintained in high-glucose Dulbecco's modified Eagle's medium (DMEM). HeLa cells were cultured in low-glucose DMEM. Media contained fetal calf serum (10%), L-glutamine (2.9  $\text{mg mL}^{-1}$ ), streptomycin (1  $\text{mg mL}^{-1}$ ), and penicillin (1000  $\text{units mL}^{-1}$ ). L929 cells were cultured in RPMI 1640 medium with newborn calf serum (5%), L-glutamine (2.9  $\text{mg mL}^{-1}$ ), streptomycin (1  $\text{mg mL}^{-1}$ ), and penicillin (1000  $\text{units mL}^{-1}$ ). All cells were cultured at 37 °C in water-saturated air supplemented with 5%  $\text{CO}_2$ . Culture media were changed every 3 days. Cells were passaged once a week. Cell numbers were estimated using a cell counter (Schaerfe cell-counting system, Germany).

Cells were plated in 96-well microtiter plates at initial densities of 1000, 2000, and 4000 cells per well. The cell-culture medium was changed every 3 days. Cell growth was tested by the colorimetric MTT assay, which measures the conversion of the yellowish water-soluble tetrazolium salt to a water-insoluble purple formazan product within viable breathing cells as a proxy of cell number and viability. The water-insoluble formazan was dissolved in a solvent mixture (100  $\mu\text{L}$ ) consisting of isopropanol (80  $\mu\text{L}$ ) with hydrochloric acid (0.04  $\mu\text{M}$ ) and 3% sodium dodecyl sulfate (20  $\mu\text{L}$ ). Absorption of the samples was measured with a spectrophotometer at 584 nm. The amount of formazan produced is directly proportional to the number of living cells in the well. MTT assays were performed every day after seeding until day 8. All experiments were carried out in triplicate.

The cytotoxicity of nanoparticles in various cell types was determined by the MTT assay. Cytotoxicity was measured in both the logarithmic and stationary phase of cell growth. For cytotoxicity measurements in the logarithmic phase, each cell line was incubated for 72 h in 96-well microtiter plates before adding the nanoparticles. Fresh medium containing increasing concentrations of nanoparticles was added to each well and the cells were incubated for another 48 h. For cytotoxicity measurements in the stationary phase, each cell line was incubated for 7 days before the addition of nanoparticles. Fresh medium containing various concentrations of nanoparticles was added and cells were incubated for another 48 h. Phosphate-buffered saline (PBS, 10  $\mu\text{L}$ ) containing MTT (5  $\text{mg mL}^{-1}$ ) was dispensed into each well and the plates were incubated for 2 h. Formazan was solubilized and measured as described under cell growth. A graphic illustration of the time schedule is given in Figure 2. The concentrations of materials were rechecked by AAS after completion of the experiments on the authentic samples.

$\text{IC}_{50}$  values were calculated by using a four-parameter logistic equation. Data were plotted as a sigmoidal dose-response

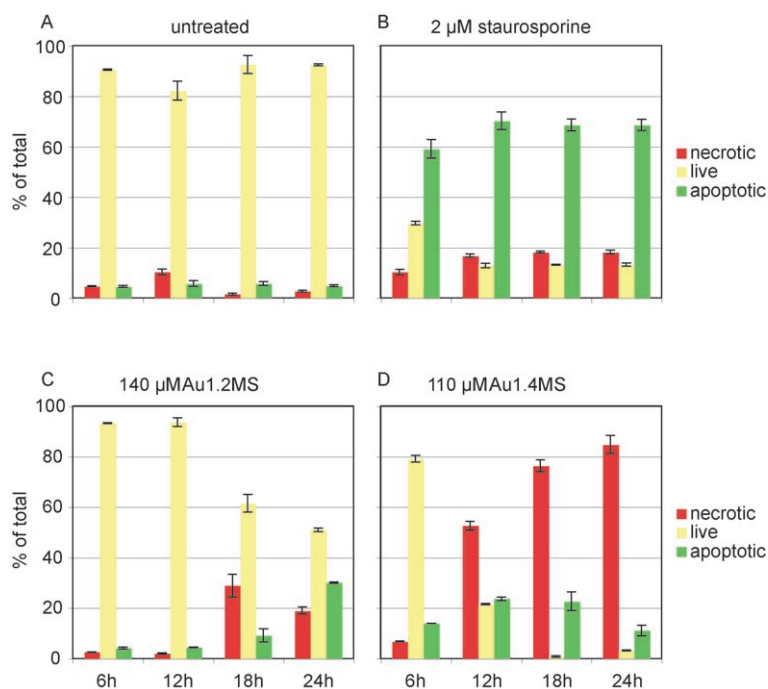


**Figure 6.** Determination of live, apoptotic, and necrotic HeLa cells untreated or treated with the indicated compounds for 6, 12, 18, and 24 h. Cells were analyzed by aV/PI double staining and flow cytometry. The proportion of live, apoptotic, and necrotic cells was determined as detailed in Figure 5. Depending on the material endocytosed, the HeLa cells showed no cell death (untreated, A), predominantly apoptosis (staurosporine, B), slow cell death with equal proportions of apoptosis and necrosis (C), or rapid cell death with transient apoptosis and predominantly necrosis (D).

curve with variable slope using GraphPad PRISM software. For each material, the  $IC_{50}$  values were determined from triplicate wells during both the stationary and logarithmic cell growth phases.  $IC_{50}$  values derived from logarithmic cell growth were routinely repeated in three independent experiments with almost identical results.

**Quantification of apoptotic and necrotic cells with fluorescence-activated cell sorting (FACS):** To measure apoptosis, HeLa cells were seeded into 96-well plates (2000 cells/well). Then cells were incubated for 72 h at 37 °C with 5%  $CO_2$  before the addition of nanoparticles. After 72 h Au1.4MS (110  $\mu M$ ) was applied. After 30 h of incubation, the medium was removed and the cells were washed twice with binding buffer followed by the addition of fluorescein isothiocyanate (FITC)-labeled aV (1  $\mu L$ , 1  $mg mL^{-1}$ ; Responsif, Erlangen, Germany) per well. The cells were incubated at room temperature on the shaker (100 rpm) for 15 min. Thereafter, PI stock solution (5  $\mu L$ , 750  $\mu M$ ) was added to each well and cells were further incubated for 5 min before one final wash in binding buffer. For each experiment, untreated cells served as a negative control and cells incubated for 5 h with staurosporine (2  $\mu M$ ) served as a positive control.

HeLa cells were incubated in 96-well plates until 80% confluent. Gold nanoparticles were added and the cells were further incubated at 37 °C with 5%  $CO_2$ . FACS analysis was performed after 1, 12, 18, and 24 h. Cells were trypsinized and collected in FACS analysis tubes. Cells were washed twice with cold PBS and resuspended in binding buffer in a final volume of 100  $\mu L$ . Then aV-FITC (1  $\mu L$ , 1  $mg mL^{-1}$ ) was added. The cells were incubated at room temperature on the shaker (100 rpm) for 15 min in dark-

ness. After this time, PI stock solution (4  $\mu L$ , 750  $\mu M$ ) was added to each tube and the cells were further incubated for 5 min before a final binding buffer wash. For each experiment, untreated cells served as a negative control. Cells incubated with staurosporine (2  $\mu M$ ) served as a positive control; 50 000 cells were counted per sample. FACS results were analyzed by CELL-Quest software (Becton-Dickinson).

**TEM:** HeLa cells were incubated in Lab-Tek II chamber slides until 80% confluence. Gold nanoparticles were added and the cells were incubated at 37 °C with 5%  $CO_2$ . After 1, 6, 12, 24 h, cells were washed twice with cold PBS, fixed in 3% glutaraldehyde for 48 h, and post-fixed in 1% osmium tetroxide. After fixation, specimens were rinsed with 8.5% sucrose and distilled water, and dehydrated in a graded series of 30, 50, 70, and 90%

ethanol and three times in 100% ethanol, for 10 min each. Samples were embedded in a mixture of EPON resin in propylene oxide polymerized at 37 °C. For optical microscopy, semithin sections (1  $\mu m$ ) were prepared and stained with methylene blue. Ultrathin sections for TEM were prepared with a diamond knife, collected on copper grids, and contrasted with uranyl acetate and lead citrate. Samples were analyzed using an EM400T transmission electron microscope (Philips).

## Acknowledgements

Financial support by the German Science Foundation (DFG) is gratefully acknowledged.

- [1] A. Nel, T. Xia, L. Madler, N. Li, *Science* **2006**, 311, 622.
- [2] E. E. Connor, J. Mwamuka, A. Gole, C. J. Murphy, M. D. Wyatt, *Small* **2005**, 1, 325.
- [3] C. M. Goodman, C. D. McCusker, T. Yilmaz, V. M. Rotello, *Bioconjugate Chem.* **2004**, 15, 897.
- [4] N. Pernodet, X. Fang, Y. Sun, A. Bakhtina, A. Ramakrishnan, J. Sokolov, A. Ulman, M. Rafailovich, *Small* **2006**, 2, 766.
- [5] H. Yi, J. Leunissen, G. Shi, C. Gutekunst, S. Hersch, *J. Histochem. Cytochem.* **2001**, 49, 279.
- [6] A. G. Tkachenko, H. Xie, Y. Liu, D. Coleman, J. Ryan, W. R. Glomm, M. K. Shipton, S. Franzen, D. L. Feldheim, *Bioconjugate Chem.* **2004**, 15, 482.

- [7] N. L. Rosi, D. A. Giljohann, C. S. Thaxton, A. K. Lytton-Jean, M. S. Han, C. A. Mirkin, *Science* **2006**, *312*, 1027.
- [8] S. L. De Wall, C. Painter, J. D. Stone, R. Bandaranayake, D. C. Wiley, T. J. Mitchison, L. J. Stern, B. S. DeDecker, *Nat. Chem. Biol.* **2006**, *2*, 197.
- [9] Y. Liu, W. Meyer-Zaika, S. Franzka, G. Schmid, M. Tsoli, H. Kuhn, *Angew. Chem.* **2003**, *115*, 2959; *Angew. Chem. Int. Ed.* **2003**, *42*, 2853.
- [10] M. Tsoli, H. Kuhn, W. Brandau, H. Esche, G. Schmid, *Small* **2005**, *1*, 841.
- [11] B. D. Chithrani, A. A. Ghazani, W. C. Chan, *Nano Lett.* **2006**, *6*, 662.
- [12] R. Shukla, V. Bansal, M. Chaudhary, A. Basu, R. R. Bhone, M. Sastry, *Langmuir* **2005**, *21*, 10644.
- [13] F. Wen, U. Englert, M. Homberger, U. Simon, *Z. Anorg. Allg. Chem.* **2006**, 2159.
- [14] G. Schmid, N. Klein, L. Korste, U. Kreibitz, D. Schonauer, *Polyhedron* **1988**, *7*, 605.
- [15] G. Schmid, M. Baumle, N. Beyer, *Angew. Chem.* **2000**, *112*, 187; *Angew. Chem. Int. Ed.* **2000**, *39*, 181.
- [16] G. Schmid, R. Pfeil, R. Boese, F. Bandermann, S. Meyer, G. H. M. Calis, J. W. A. van der Velden, *Chem. Ber.* **1981**, *114*, 3634.
- [17] G. Schmid, *Clusters and Colloids—From Theory to Applications*, Wiley-VCH, Weinheim, Germany, **1994**.
- [18] G. Schmid, R. Pugin, T. Sawitowski, U. Simon, B. Marler, *Chem. Commun.* **1999**, 1303.
- [19] <http://www.strem.com>.
- [20] J. Turkevitch, P. C. Stevenson, J. Hillier, *Discuss. Faraday Soc.* **1951**, *11*, 55.
- [21] G. Schmid, A. Lehnert, *Angew. Chem.* **1989**, *101*, 773; *Angew. Chem. Int. Ed. Engl.* **1989**, *28*, 780.
- [22] F. Joó, J. Kovács, Á. Kathó, A. Bényei, T. Decuir, D. Darensbourg, A. Miedaner, D. Dubois, *Inorg. Synth.* **1998**, *32*, 1.
- [23] P. L. Bellon, F. Cariati, M. Manasser, L. Naldini, M. Sansoni *J. Chem. Soc., Chem. Commun.* **1971**, 1423.
- [24] J. W. A. Van der Velden, J. J. Bour, W. P. Bosman, J. H. Noordik, *Inorg. Chem.* **1983**, *22*, 1913.
- [25] K. P. Hall, D. M. P. Mingos, *Prog. Inorg. Chem.* **1984**, *32*, 237.

Received: May 29, 2007

Revised: August 27, 2007